Journal of
Marine Science and Engineering

MDPI

Article

A Method for Full-Depth Sound Speed Profile Reconstruction Based on Average Sound Speed Extrapolation

Wei Zhang, Shaohua Jin *, Gang Bian, Chengyang Peng and Haixing Xia

Department of Oceanography and Hydrography, Dalian Naval Academy, Dalian 116018, China; 18590361852@163.com (W.Z.); trighosts@163.com (G.B.); 18908414801@163.com (C.P.); a1466448779@163.com (H.X.)
* Correspondence: jsh_1978@163.com

Abstract: The speed of sound in seawater plays a crucial role in determining the accuracy of multibeam bathymetric measurements. In deep-sea multibeam measurements, the challenge of inadequate longitudinal coverage of sound speed profiles arises from variations in seafloor topography, meteorological conditions, measurement equipment, and operational efficiency, resulting in diminished measurement precision. Building upon the EOF (Empirical Orthogonal Function), a method employed to analyze spatiotemporal data such as sound speeds, this paper addresses the limitations of the EOF method caused by the shallowest sampling depth of the sound speed profile samples. It proposes two methods for EOF reconstruction of measured sound speed profiles extended to full water depth by splicing measured sound speed profiles at non-full water depths with historical average sound speed profiles of the surveyed sea area. Specially, Method 2 introduces the latest metaheuristic optimization algorithm, CPO (Crested Porcupine Optimizer), which exhibited superior performance on multiple standard test functions in 2024. The study reconstructs randomly sampled measured sound speed profiles using the two proposed methods and commonly employed substitution and splicing methods, followed by a comparative analysis of the experimental outcomes. At a sampling depth of 200 m, Method 2 demonstrates performance superior to other methods, with RMSE, MAE, MAPE, and R^2 values of 0.9511 m/s, 0.8492 m/s, 0.0566%, and 0.9963, respectively. Method 1 yields corresponding values of 0.9594 m/s, 0.8492 m/s, 0.0568%, and 0.9962, respectively. Despite its slightly inferior performance compared with Method 2, it offers substantial advantages over the substitution and splicing methods. Varying the sampling depth of measured sound speed profiles reveals that Methods 1 and 2 exhibit inferior reconstruction performance in shallow water compared with the substitution and splicing methods. Nevertheless, when the sampling depth surpasses the depth range of initial spatial modes with abrupt variations, both methods achieve notably higher reconstruction accuracy compared with the substitution and splicing methods, reaching a stabilized state. Sound ray tracing reveals that the reconstructed sound speed profiles from both methods meet the stringent accuracy standards for bathymetric measurements, achieving an effective beam ratio of 100%. The proposed methods not only provide rapid reconstruction of sound speed profiles, thereby improving the efficiency of multibeam bathymetric surveys, but also provide references for the reasonable determination of sampling depths of sound speed profiles to ensure reconstruction accuracy, demonstrating practical application value.

Keywords: multibeam bathymetry; reconstruction of sound speed profile; average sound speed profile; EOF; CPO; sound ray tracing

check for updates

Citation: Zhang, W.; Jin, S.; Bian, G.; Peng, C.; Xia, H. A Method for Full-Depth Sound Speed Profile Reconstruction Based on Average Sound Speed Extrapolation. *J. Mar. Sci. Eng.* **2024**, *12*, 930. https://doi.org/10.3390/jmse12060930

Received: 28 April 2024
Revised: 21 May 2024
Accepted: 29 May 2024
Published: 31 May 2024

Copyright: © 2024 by the authors. Licensee MDPI, Basel, Switzerland. This article is an open access article distributed under the terms and conditions of the Creative Commons Attribution (CC BY) license (https://creativecommons.org/licenses/by/4.0/).

1. Introduction

The precision of multibeam seafloor topography measurements is contingent upon numerous factors, among which the speed of sound in seawater emerges as pivotal. Principally, it impacts the computation of seafloor measurement point coordinates by shaping sound ray trajectories, and the accuracy and dependability of measurement outcomes

hinge directly upon the correctness of the sound speed profile [1–5]. Conventionally, the sound speed profile manifests as a function of depth-dependent sound velocity, mirroring the longitudinal variations in sound speed structure within the local marine domain, chiefly dictated by marine environmental factors like seawater temperature, salinity, and pressure [6,7]. Due to the influence of factors such as solar radiation, precipitation, ocean currents, tides, internal waves, and others on the marine environment, the sound speed profile exhibits complex spatiotemporal variations [8]. Therefore, it is necessary to timely acquire accurate sound speed profiles of the measured sea area for real-time or post-survey correcting of multibeam survey data.

Currently, there are two main methods for measuring seawater sound speed: direct methods and indirect methods [9,10]. Direct methods involve using equipment such as AML Minos SVP or SVP-plus sound velocity profilers to directly obtain sound speed profiles in seawater through fixed-point measurements. Indirect methods utilize devices like CTD, XCTD, XBT, MVP, etc., to obtain temperature and salinity information in seawater through survey or fixed-point measurements, calculating the sound speed in seawater using suitable empirical formulas. When conducting deep-sea bathymetric surveys, whether using direct methods or indirect methods, the following situations are often encountered, leading to the inability to obtain a complete sound speed profile for the entire sea depth.

(1) Complex variations in seafloor topography in the surveyed sea area. This includes two situations. First, during the navigation progress of a survey vessel from a dock to deep sea through shallow waters. The water depth gradually increases, leading to the collected sound speed profile not achieving full coverage of the water's depth. Second, complexity in the topographical changes within the surveyed sea area. If the selection of sound profile stations is unreasonable (such as choosing points in shallow waters), it results in an insufficient vertical coverage range of the sound speed profile, leading to incomplete post-survey sound speed corrections.

(2) Insufficient effective detection depth of equipment. The effective detection depth of XBT is approximately 800 m, while that of XCTD is around 1100 m. For deep-sea topography measurements in water depths of over a thousand meters, the detection depth of such survey equipment falls far short of the requirements for comprehensive coverage of an area's topography measurements.

(3) Operational inefficiency. The "Hydrographic Survey Specification of China" stipulates that sound speed acquisition operations should ideally be conducted daily. When measuring sound speed using CTD or sound velocity profilers to obtain a sound speed profile of the entire water depth in areas in which the sea is 4000 m deep, a conservative estimate indicates that it would take 3–4 h [11], from stopping the vessel to deploying and then recovering the equipment, to obtain a profile. Operational efficiency is thus low.

(4) Meteorological conditions. During operations, interruptions due to high winds and waves at sea are common, leading to the inability to obtain a complete sound speed profile of the entire sea depth.

The National Oceanic and Atmospheric Administration (NOAA) of the United States clearly stipulates that during the measurement process, the actual non-full water depth sound speed profile must be vertically extended to the maximum depth of the actual field water depth [12]. Field practices have found that using non-full water depth sound speed profiles for speed corrections can cause the depth measurement strips to exhibit undulations, impacting the accurate representation of seafloor topography [13]. Therefore, reconstructing sound speed profiles of the full water depth using measured profiles is of significant importance for enhancing depth measurement accuracy and operational efficiency.

In reconstructing sound speed profiles, using mathematical means for fitting and extrapolation is a common and efficient approach, especially suitable for nearshore or offshore areas. This method is particularly applicable because, compared to shallow water areas such as estuaries and coastlines where sound speed variations are irregular, the sound speed variations in nearshore or offshore waters exhibit certain regularities and can be to some extent predicted [14]. Wu Tongyuan et al. [15] employed a polynomial

model to fit and extrapolate the measured sound speed profiles. The results showed that, among various extrapolations based on fourth-order fitting, third-order polynomial extrapolation still maintained high accuracy at relatively long distances. This method is highly effective when dealing with constant sound speed gradients or minor gradient changes. However, it may lead to significant errors when encountering sudden features such as a sound channel axis. To represent the sound speed structures of different water layers such as the mixed layer, thermocline, deep sound channel layer, and deep isothermal layer, structured parameter models of sound speed profiles are commonly used. Munk [16] proposed a sound speed profile model for mid-latitude deep-sea sound channels using an exponential expression based on the layering characteristics of deep-sea density structures. Davis et al. [17] proposed the Generalized Digital Environmental Model (GDEM), which describes temperature and salinity profiles in seawater using more complex function combinations. Building upon analytical function models such as Munk and GDEM, Zhang Xu et al. [18] proposed a 9-parameter sound speed profile model, LSSPM (Layered Sound Speed Profile Model), which is more suitable for the Chinese nearshore environment. This model significantly reduces the number of parameters while integrating the advantages of both Munk and GDEM models, thereby improving the efficiency of describing sound speed structures. Although parameterized models facilitate the expression of sound speed profiles, their idealized representation cannot fully describe complex marine environments.

EOF is a widely used method for representing sound speed profiles. It can accurately represent the complex variations of sound speed profiles using the first few eigenvectors obtained by EOF decomposition and a small number of parameters. Research by LeBlanc et al. [19] shows that EOF is the most effective basis function for describing sound speed profiles. Park et al. [20] demonstrated that only a few representative empirical orthogonal functions are needed to represent the main differences in the sound field of a marine area. Shen Yuanhai et al. [21] demonstrated the feasibility of using EOF to represent shallow water sound speed profiles using data from the South China Sea. Sun Wenchuan et al. [22] demonstrated the effectiveness of the EOF method in representing sound speed profiles. He Li et al. [23] represented sound speed profiles in the East China Sea using a small number of empirical orthogonal functions. Zhang Zhenmai et al. [24] reconstructed the sound speed profile of the entire ocean depth using finite-depth measured sound speed data combined with the EOF method. Zhang Wei et al. [25] extrapolated incomplete temperature and salinity profiles, calculated sound speed using empirical formulas, selected three sound speed points with significant changes, solved EOF coefficients, and reconstructed the entire ocean depth sound speed profile using the first three EOFs. Cheng Fang et al. [26] used a small amount of full-depth sound speed profile sampling data in the surveyed area as a basis and the EOF method to extrapolate the sound speed profiles that were not sampled to full depth. Although the EOF method can simplify the representation of sound speed profiles, it is not suitable for extrapolating non-full-depth sound speed profiles because this method is limited by the minimum sampling depth of the sample data.

Inspired by the research results of Yang Fan et al. [27] and based on the reconstruction of sound speed profiles using EOF decomposition, this paper addresses the practical problem of the EOF method's inability to extend measured non-full-depth sound speed profiles to full depth. It considers splicing the full-depth historical average sound speed profile of an area with a measured sound speed profile of that area to extend the measured profile to full depth. On this basis, two methods are proposed to reconstruct the measured sound speed profile. One is to combine the extended measured sound speed profile with the sample data of historical sound speed profiles to form a new sound speed matrix, perform EOF analysis on this matrix, and reconstruct the extended measured sound speed profile. The other is to directly perform an EOF analysis on the matrix of historical sound speed profiles and use the rapid optimization ability of the CPO algorithm to find the optimal reconstruction coefficients for the extended measured sound speed profile. For convenience, these two methods are respectively referred to as Method 1 and Method 2.

This article is organized as follows: In Section 1, the significance of sound speed profile reconstruction is briefly introduced, along with an overview of existing methods and the associated challenges. Section 2 provides a detailed explanation of EOF, highlighting the novel approach proposed in this study. The experimental setup, including the data utilized, the experimental process, and the evaluation metrics for the results, is presented in Section 3. Section 4 presents a comprehensive analysis of the experimental results, discussing the findings in detail. Finally, in Section 5, the relevant work discussed in the article is summarized and potential avenues for future research are proposed.

2. Methods

2.1. The Principle of EOF

2.1.1. EOF Decomposition and Reconstruction of Sound Speed Profiles

The EOF analysis, also known as Principal Component Analysis (PCA) or Eigenvector Analysis, was initially introduced by the statistician Karl Pearson [28] in 1901. It is a method for analyzing the structure of a matrix of data and extracting its primary features. In the 1950s, Lorenz introduced the EOF method to the field of atmospheric science. This method can decompose meteorological field elements that vary over time into orthogonal spatial modes and time coefficients, effectively extracting the primary patterns of variation and their time series from the data. It is an important tool in the study of large-scale circulation, ocean dynamics, climate change, and other fields. The fundamental process of EOF decomposition and reconstruction of sound speed profiles is illustrated in Figure 1.

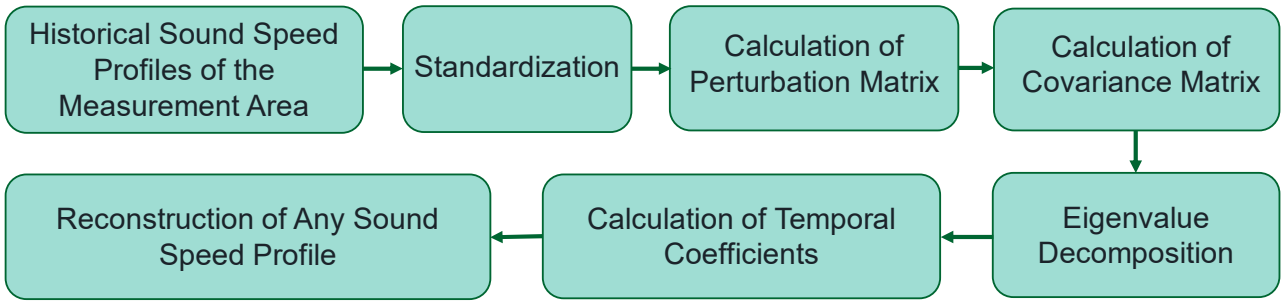

Figure 1. Process of EOF decomposition and reconstruction of sound speed profiles.

Specifically, to decompose the sound speed profiles using the EOF method, first, the N sound speed profiles collected at different times in the measured sea area need to be interpolated in the depth direction into M standard layers, resulting in the standardized sound speed matrix $C_{M\times N}$:

$$C_{M\times N} = \begin{bmatrix} c_{11} & c_{21} & \cdots & c_{N1} \\ c_{12} & c_{22} & \cdots & c_{N2} \\ \vdots & \vdots & \vdots & \vdots \\ c_{1M} & c_{2M} & \cdots & c_{NM} \end{bmatrix} \tag{1}$$

Here, c_{ij} represents the sound speed value corresponding to the j water layer of the i sound speed profile. Each row comprises the sound speed values of N sound speed profile samples at the same water layer, and each column represents the sound speed values of the same sound speed profile at different water layers. By averaging each row of the standardized sound speed matrix, the historical average sound speed profile $\overline{C}_{M\times 1} = \begin{bmatrix} \overline{c_1} & \overline{c_2} & \cdots & \overline{c_M} \end{bmatrix}^T$ is obtained, where $\overline{c_i}$ represents the average sound speed value of different sound speed profiles at the same water layer. The average sound speed profile is expanded into N columns by replicating it column-wise, resulting in the average sound

speed matrix $\overline{C}_{M\times N}$. Subtracting the average sound speed matrix from the standardized sound speed matrix, the perturbation matrix (anomalies matrix) $\Delta C_{M\times N}$ is obtained:

$$\Delta C_{M\times N} = C_{M\times N} - \overline{C}_{M\times N} \tag{2}$$

The covariance matrix $R_{M\times M}$ of the perturbation matrix is computed as:

$$R_{M\times M} = \frac{1}{N}\Delta C_{M\times N}\Delta C_{M\times N}^{T} \tag{3}$$

The essence of EOF analysis lies in analyzing the covariance matrix of the data, obtaining the eigenvalues and corresponding eigenvectors of the covariance matrix through eigen decomposition. Each eigenvector represents a spatial mode, and its corresponding eigenvalue indicates the importance of that mode to the entire dataset. Perform eigen decomposition on $R_{M\times M}$:

$$R_{M\times M}F_{M\times M} = D_{M\times M}F_{M\times M} \tag{4}$$

Here, $D_{M\times M}$ represents the matrix of eigenvalues of the covariance matrix. After arranging the eigenvalues in descending order, the following is obtained:

$$D_{M\times M} = diag\begin{bmatrix}\lambda_1 & \lambda_2 & \cdots & \lambda_M\end{bmatrix} \tag{5}$$

$F_{M\times M}$ represents the matrix of eigenvectors corresponding to the eigenvalue matrix. After synchronous adjustment with the eigenvalue matrix, it can be expressed as follows:

$$F_{M\times M} = \begin{bmatrix}f_1 & f_2 & \cdots & f_k\end{bmatrix} \tag{6}$$

Here, $f_k(k = 1, 2, \ldots, M)$ represents the k order spatial mode.

After performing EOF decomposition on the historical sound speed profiles in the measurement area, any sound speed profile within the region can be reconstructed using the leading spatial modes.

$$c(z) = \overline{c}(z) + \sum_{i=1}^{K}\alpha_i f_i(z), K = 1, 2, \ldots, M \tag{7}$$

Here, $c(z)$ represents the reconstructed sound speed profile, $\overline{c}(z)$ represents the average sound speed profile, z represents the depth of each standard layer, $f_i(z)$ represents the i order spatial mode, α_i represents the corresponding time coefficient of the i order spatial mode, and K represents the order of the selected spatial modes.

By moving $\overline{c}(z)$ from Equation (7) to the left side and expressing it in matrix form, $\Delta C_{M\times N}$ is then obtained as follows:

$$\Delta C_{M\times N} = C_{M\times N} - \overline{C}_{M\times N} = F_{M\times K}A_{K\times N} \tag{8}$$

Thus, the matrix of time coefficients $A_{K\times N}$ is obtained as follows:

$$A_{K\times N} = F_{M\times K}^{T}\Delta C_{M\times N} = \begin{bmatrix}a_1 & a_2 & \cdots & a_N\end{bmatrix}_{K\times N} \tag{9}$$

Here, $a_i = \begin{bmatrix}a_i(1) & a_i(2) & \cdots & a_i(K)\end{bmatrix}^T$ represents the time coefficient corresponding to the i-th sound speed profile. After obtaining the time coefficients, any sound speed profile within the measurement area can be reconstructed according to Equation (7).

2.1.2. Variance Contribution Ratio of Spatial Modes

In EOF analysis, the variance contribution ratio is a crucial concept employed to quantify the contribution of each order of spatial modes to the entire sound speed field, with the calculation formula as follows:

$$\sigma_i = \frac{\lambda_i}{\sum_{i=1}^{M} \lambda_i} \times 100\% \tag{10}$$

Here, σ_i represents the variance contribution ratio of the i order spatial mode, λ_i denotes the eigenvalue corresponding to the i order spatial mode (in descending order), and M is the total number of eigenvalues.

The cumulative variance contribution ratio of the first K order spatial modes is given by:

$$w(K) = \frac{\sum_{i=1}^{K} \lambda_i}{\sum_{j=1}^{M} \lambda_j} \tag{11}$$

When reconstructing sound speed profiles, concerning the selection of spatial mode orders, Davis [29] pointed out that if the cumulative variance contribution ratio of the first K order spatial modes exceeds or equals 95%, then it is considered that the main information of the sound speed field in that region can be precisely delineated by these K order spatial modes.

2.2. Method 1

Illustrated in Figure 2, the fundamental process of Method 1 for a designated measurement sea area unfolds as follows:

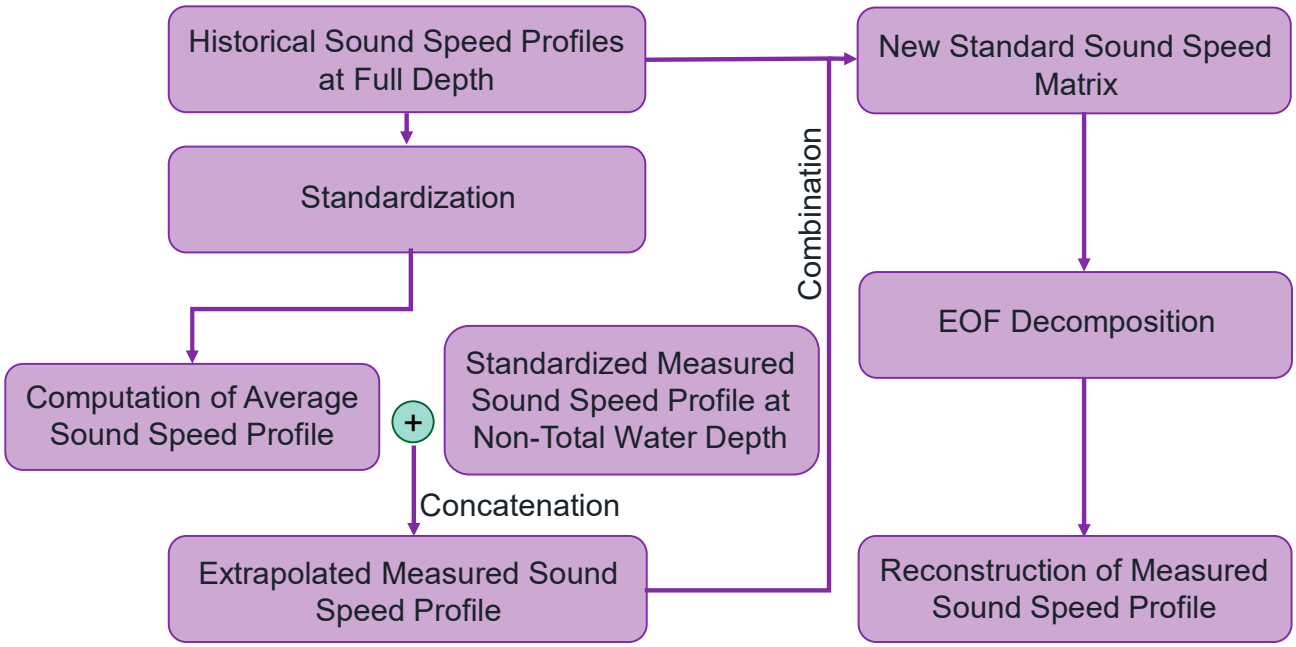

Figure 2. Basic process of Method 1.

(1) Choose historical full-depth sound speed profiles obtained at various stations and times within the measurement sea area (if temperature-salinity-depth (pressure) data are available at these stations, suitable empirical formulas should be employed to convert them into sound speed values). The choice of historical sound speed profiles limits the precision of sound speed profile EOF reconstruction. If there are significant differences in the properties of sound speed variations within the measurement area, it may lead to a decrease in the accuracy of sound speed profile EOF reconstruction, failing to accurately reflect the real sound speed variation. At present, there is no specific discussion of the spatiotemporal

range concerning the selection of historical sound speed profiles. Although a narrower spatiotemporal range yields superior reconstruction outcomes, for extensive deep-sea terrain measurements, the reconstruction efficiency will be significantly diminished. In pertinent literature, numerous researchers confine the spatial scope within an interval of $5^{\circ} \times 5^{\circ}$, and a temporal scope within quarterly periods. Of course, the spatiotemporal range for selecting historical sound speed profiles should also be reasonably determined according to the actual hydrological conditions of the measurement sea area. If drastic changes occur in the hydrological elements within the measurement area, the spatial range can be narrowed down to $3^{\circ} \times 3^{\circ}$, and the temporal range limited to monthly intervals, concurrently augmenting the number of historical sound speed profile samples in the measurement area.

(2) Employ the Akima interpolation method [30,31] to interpolate the historical sound speed profiles chosen in step (1) into standard sound speed profiles with uniform intervals based on the specified depth interval, thereby assembling a matrix of standard sound speed profiles. To reconstruct the measured non-full-depth sound speed profiles, employ the same method to interpolate them to their maximum measured depth.

(3) Compute the average value of the matrix of standard sound speed profiles row-wise to derive the historical average sound speed profile.

(4) Determine the disparity between the sound speed at the concluding depth of the sound speed profile to be reconstructed and the sound speed at the depth corresponding to the identical depth of the average sound speed profile. Add this difference to the average sound speed profile from this depth to the last depth corresponding to it, then truncate this part of the average sound speed profile and concatenate it with the measured sound speed profile to be reconstructed to obtain an extrapolated measured sound speed profile.

(5) Combine the extrapolated measured sound speed profile with the original matrix of standard sound speed profiles to form a new matrix of sound speed profiles. In accordance with Section 2.1, perform EOF decomposition on this matrix to obtain spatial modes and temporal coefficients. Taking 95% as the minimum threshold, calculate the cumulative variance contribution ratio of the first K order spatial modes to determine the minimum number of orders of spatial modes necessary to reconstruct the sound speed profile, and then reconstruct the measured sound speed profile according to Equation (7).

2.3. Method 2

2.3.1. CPO

CPO is a novel metaheuristic intelligent optimization algorithm proposed by Abdel-Basset et al. in 2024 [32]. This algorithm emulates a plethora of defense behaviors exhibited by the crested porcupine, rendering it especially conducive for tackling large-scale optimization problems. The defense mechanism of the crested porcupine is categorized into four escalating types: visual, auditory, olfactory, and physical attacks. Within the framework of the CPO algorithm, the search space is depicted as illustrated in Figure 3, where regions A, B, C, and D symbolize four distinct defense stages. Region A represents the first defense stage, where the crested porcupine raises and flaps its quills upon recognizing the predator, implementing the first defense strategy, namely visual defense. Region B represents the second defense stage, indicating that the predator is not deterred by the first defense mechanism and is moving toward the prey. At this point, the crested porcupine starts making noise to threaten the predator, implementing the second defense mechanism, namely auditory defense. Region C represents the third defense stage, where if the predator is not deterred by the first and second defense mechanisms and continues to approach the crested porcupine, it begins to secrete odors and spread them around to dissuade the predator from getting closer, implementing the third defense mechanism, namely olfactory defense. Region D represents the fourth defense stage, where the crested porcupine starts to physically attack the predator. The initial two defense mechanisms are affiliated with the exploratory behavior of CPO, whereas the subsequent two defense mechanisms

are aligned with the exploitative behavior of CPO. The mathematical simulation of each defense mechanism is detailed in [32] and will not be reiterated in this paper.

It is noteworthy that the algorithm introduces a highly innovative strategy termed as the "population cyclic reduction technique", wherein solely threatened crested porcupines trigger their defense mechanisms rather than the entire population. Test results suggest that the algorithm demonstrates markedly superior performance in contrast to other commonly employed optimization algorithms.

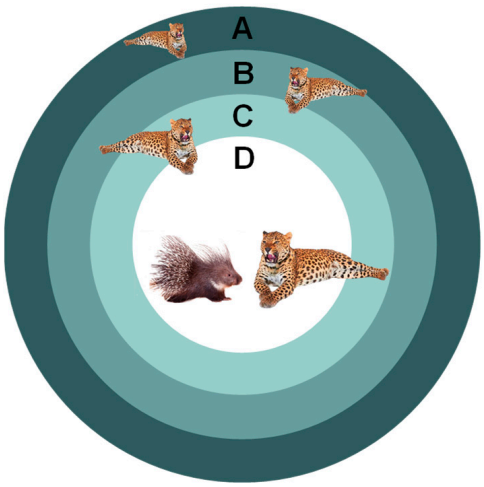

Figure 3. Visualization of CPO search space.

2.3.2. Basic Process

The objective of employing the CPO algorithm is to leverage its rapid convergence advantage in order to swiftly obtain optimal EOF reconstruction coefficients. As depicted in Figure 4, the basic process for Method 2, applied to the designated measurement marine area, is outlined as follows:

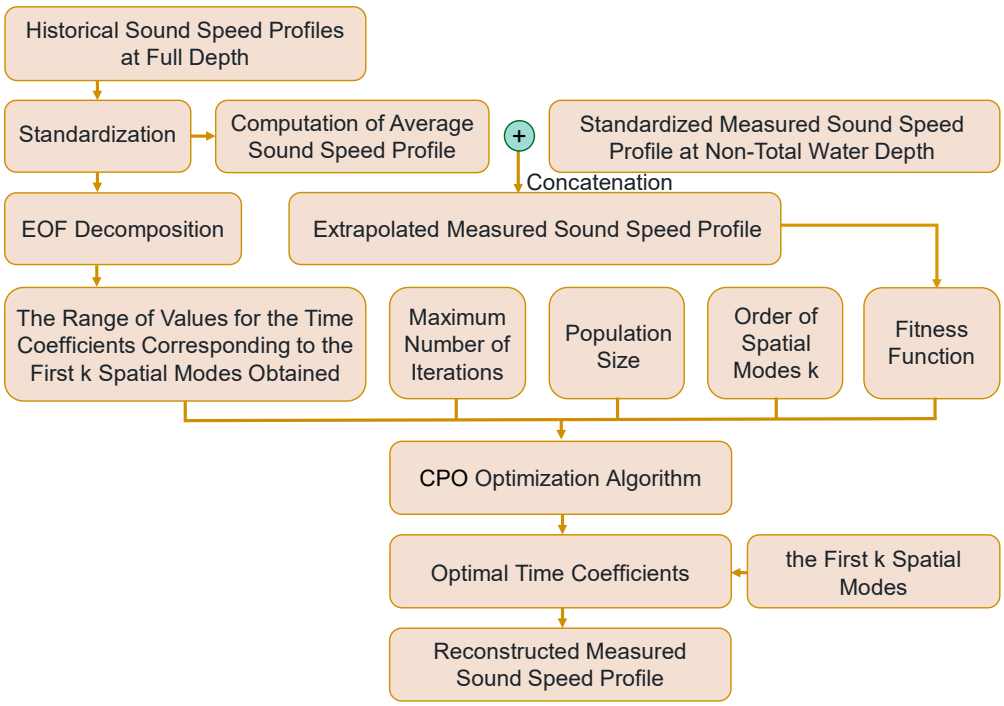

Figure 4. Basic process of Method 2.

(1)–(4) follow the steps outlined in Section 2.2 (1)–(4).

(5) Conduct EOF decomposition on the standard sound speed profile matrix to extract spatial modes and temporal coefficients. Compute the cumulative variance contribution rate of the first K spatial modes, with a minimum threshold of 95%, to determine the minimum number of spatial modes K involved in the reconstruction of measured sound speed profiles. This value of K serves as one of the input parameters for the CPO algorithm, termed as the problem dimension. Simultaneously, identify the maximum and minimum values of the temporal coefficients corresponding to each order of the K order spatial modes. Arrange the maximum values of the temporal coefficients in ascending order of order to form a row vector, constituting the second input parameter of the CPO algorithm, denoted as the upper bound of the search space. Similarly, arrange the minimum values of the temporal coefficients in ascending order of order to form a row vector, constituting the third input parameter of the CPO algorithm, termed as the lower bound of the search space.

(6) Analogous to other metaheuristic population-based algorithms, the CPO algorithm necessitates configuring the population size, maximum number of iterations, and fitness function.

(7) Employ the optimal temporal coefficients generated by the algorithm, in conjunction with the spatial modes derived from EOF decomposition, and employ Equation (7) to reconstruct the measured sound speed profiles.

3. Materials and Experiments

3.1. Experimental Data

The experimental data utilized in this study were sourced from the global Argo real-time ocean observing network observations, accessed from the website of the Chinese Argo Real-Time Data Center (http://www.argo.org.cn, accessed on 26 March 2024). A defined region in the Pacific Ocean (latitude 23–26° N, longitude 135–138° E) was selected as the study area. A total of 43 station measurements of temperature and salinity profiles collected during February from 2002 to 2008 were chosen as the experimental samples. One station was randomly selected as the validation station. The distribution of stations is illustrated in Figure 5.

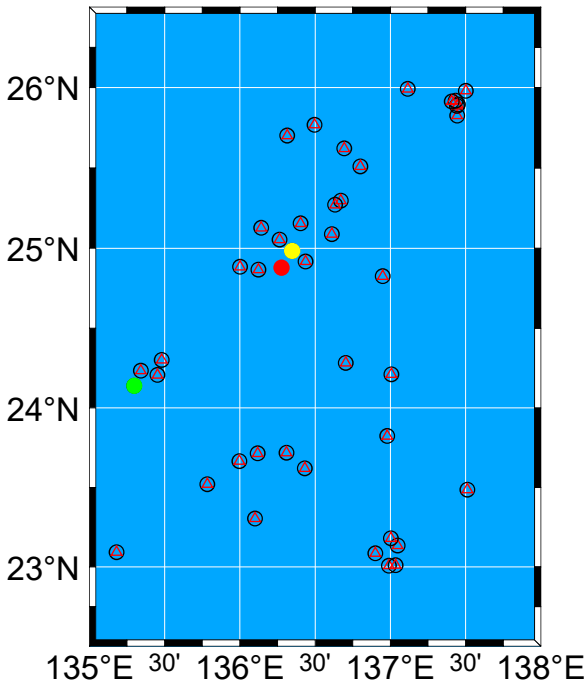

Figure 5. The distribution of the sound profile stations, where the red solid circle represents the validation station, the yellow solid circle denotes the station closest in location to the validation station, and the green solid circle indicates the station closest in measurement time to the validation station, with other points representing regular stations.

As the Argo data provide temperature and salinity information at specific oceanic points, it is necessary to employ suitable empirical formulas to convert them into sound speed data. Following the comparative analysis conducted by Zhou Fengnian et al. [33], the Mackenzi formula and the EM stratified simplified sound speed formula were found to yield satisfactory computational accuracy across the entire depth range of 1–12,000 m. Because the Mackenzie formula has a relatively simple structure and remains unchanged across various depth layers, it was ultimately selected for sound speed calculation in this study. The formula is as follows:

$$C = 1448.96 + 4.591T - 5.304 \times 10^{-2}T^2 + 2.374 \times 10^{-4}T^3 + 1.340 \times (S - 35) + 1.630 \times 10^{-2}D + 1.675 \times 10^{-7}D^2 - 1.025 \times 10^{-2}T(S - 35) - 7.139 \times 10^{-13}TD^3 \quad (12)$$

Here, C (m/s) represents sound speed, T (°C) denotes temperature, S (ppt) signifies salinity, D (m) indicates depth.

Analysis of the sound speed profile data from various stations reveals that sampling depths typically hover around 1000 m. Due to the irregular sampling intervals of Argo, interpolating the sound speed profiles to standard layers becomes necessary for EOF analysis. Hence, this study employs the Akima interpolation method to interpolate each sound speed profile from 0 m to 1000 m with a 1 m depth interval. The interpolated sound speed profiles are illustrated in Figure 6. It is apparent from the figure that the sound speed values within each profile fall within the range of 1480–1540 m/s, indicating a consistent variation in sound speed. The structure of these sound speed profiles adheres to the characteristic features of typical deep-sea sound speed profiles.

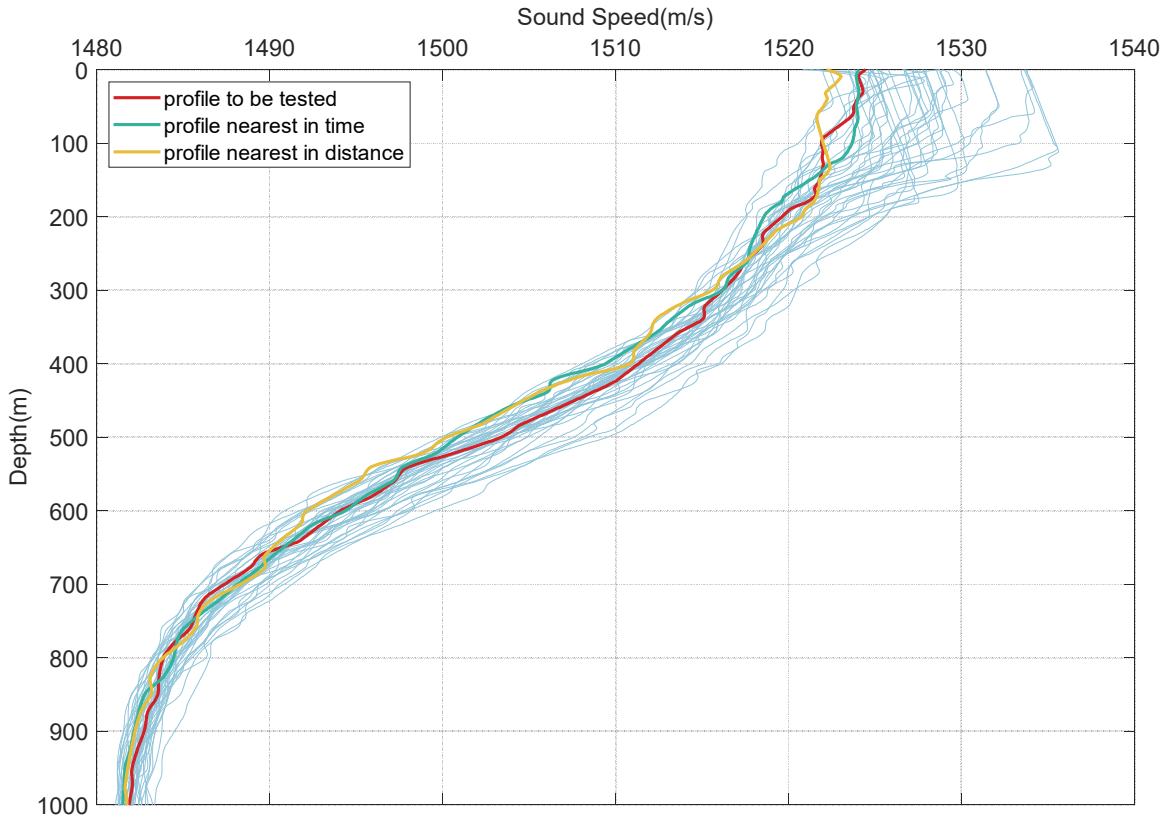

Figure 6. Sound speed profile curves for each station, where the red solid line represents the sound speed profile of the validation station, the green solid line represents the sound speed profile closest in measurement time to the validation profile, the yellow solid line represents the sound speed profile closest in measurement location to the validation profile, and the light blue solid lines represent the sound speed profiles of the remaining stations.

3.2. Experimental Process

Assuming a measured depth of 200 m for the sound speed profile, the portions of the tested profile exceeding this depth are truncated, retaining only the data up to 200 m as the target for reconstruction. The experimental process, depicted in Figure 7, involves the application of four distinct methods to reconstruct the aforementioned sound speed profile. Subsequently, an evaluation and analysis of the reconstructed results are conducted using specified metrics. Following this, simulation calculations are performed to trace ray paths based on the reconstructed sound speed profiles obtained from each method, followed by an analysis of the outcomes.

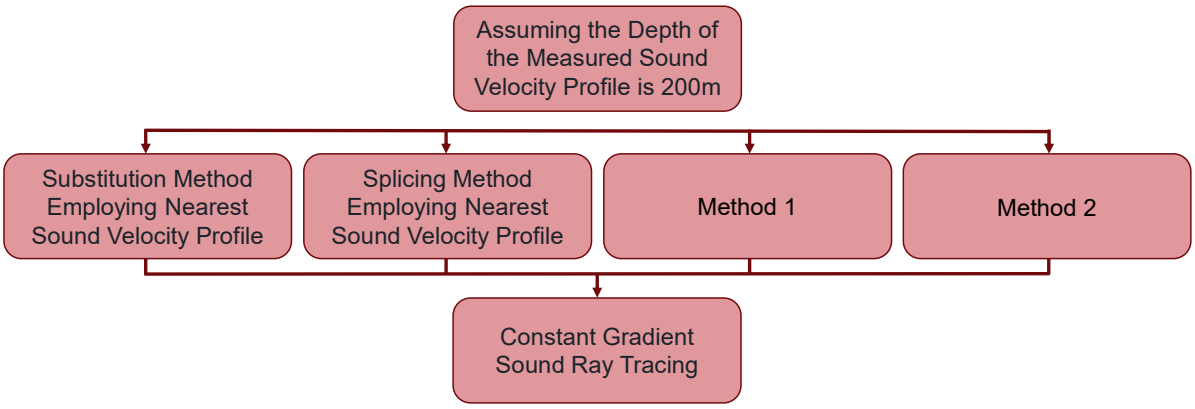

Figure 7. Experimental process.

It is pertinent to note that in practical multibeam operations, when confronted with issues such as untimely sound speed profile measurements or abrupt changes in seabed topography resulting in insufficient longitudinal coverage, operators often resort to contingency measures such as the nearest substitution method or nearest splicing method. This involves substituting the most recently measured or geographically closest sound speed profile for the current one, or cutting and splicing parts of them with the current profile to extend it. In areas with relatively stable sound speed variations, this practice not only simplifies the operation but also ensures the accuracy of sound ray tracing while extending the sound speed profile. However, in regions with complex sound speed variations, these methods may introduce significant measurement errors due to the inability to ascertain whether the sound speed variations between two points are consistent. In order to comprehensively compare the advantages and disadvantages of different methods, this study also includes these two methods as part of the experiments.

3.2.1. Reconstruction of the Measured Sound Speed Profile Using Four Methods

The nearest substitution method involves substituting the profile with the one measured closest in time or location to the current sound speed profile in use. Similarly, the nearest splicing method entails splicing the profile with the one measured closest in time or location to the current sound speed profile, using the splicing method consistent with the procedure outlined in Section 2.2, step (4), which is based on average sound speed splicing. The relevant parameters of the tested sound speed profile and the nearest (either closest in time or location) sound speed profiles are presented in Table 1.

Table 1. Relevant parameters of tested sound speed profile and nearest (time/location) sound speed profiles.

	Tested Sound Speed Profile	Sound Speed Profile Nearest in Time	Sound Speed Profile Nearest in Location
Measurement Time	15 February 2006	15 February 2006	20 February 2006
Measurement Location	24.878° N, 136.277° E	24.139° N, 135.298° E	24.983° N, 136.347° E

The overall processes of the substitution and splicing methods are straightforward and require no further elaboration. Here, the paper only focuses on providing specific explanations for the proposed methods, namely Method 1 and Method 2.

1. Method 1

(1) EOF decomposition. Combine the 42 historical sound speed profiles (excluding the tested sound speed profile) interpolated in Section 3.1 into a standard sound speed profile matrix and calculate the average value of each row to obtain the average sound speed profile. In accordance with Section 2.2, concatenate the average sound speed profile with the measured sound speed profile to obtain the sound speed profile for the entire water depth. Combine the extrapolated sound speed profile with the historical sound speed profile matrix to form a new standard sound speed matrix. In accordance with Section 2.1.1, perform EOF decomposition on this matrix to obtain the first seven order spatial modes as shown in Figure 8.

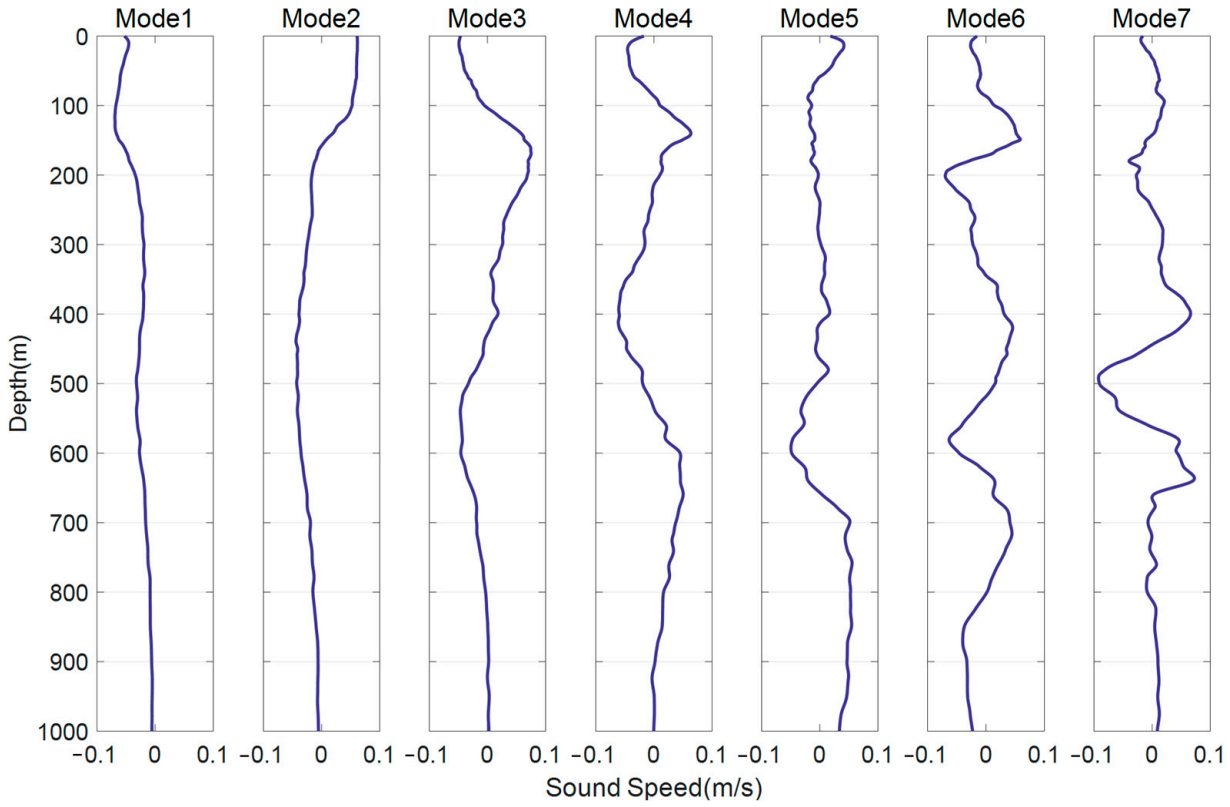

Figure 8. The first 7 order spatial modes obtained by EOF decomposition of the new standard sound speed matrix.

Analysis of Figure 8 reveals that the first seven order spatial modes (except the 5th mode) tend toward zero in depths greater than 800 m, indicating that there are basically no disturbances in the sound speed profiles in water layers deeper than 800 m, and the sound speed variations tend to stabilize. The first, third, fourth, and sixth spatial modes all exhibit extreme values (either maximum or minimum) in the depth range of 100–200 m, indicating significant variations in the sound speed profiles in this depth interval. Further analysis, in conjunction with Figure 6, reveals that compared with other depth layers, there are indeed significant differences in the sound speed profiles in this water layer.

(2) Determination of spatial mode order. Calculate the variance contribution ratio and cumulative variance contribution ratio of the first K spatial modes. The variation of the variance contribution ratio and cumulative variance contribution ratio of the first 20 spatial

modes is shown in Figure 9, and the specific values of the variance contribution ratio and cumulative variance contribution ratio of the first seven spatial modes are shown in Table 2.

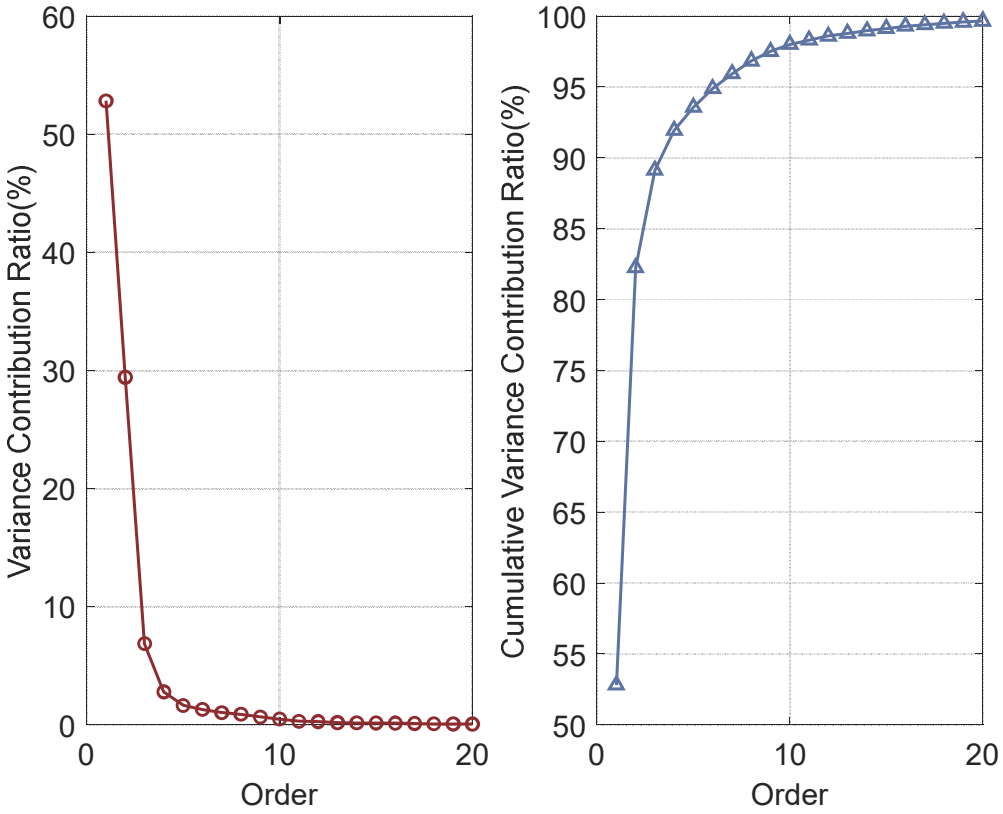

Figure 9. Variation of variance contribution ratio and cumulative variance contribution ratio of the first 20 spatial modes.

Table 2. Variance contribution ratio and cumulative variance contribution ratio of the first 7 spatial modes.

Mode	Eigenvalue	Variance Contribution Ratio (%)	Cumulative Variance Contribution Ratio (%)
1	1996.14	52.82	52.82
2	1112.03	29.43	82.25
3	260.00	6.88	89.13
4	105.77	2.80	91.93
5	62.05	1.64	93.57
6	49.51	1.31	94.88
7	39.40	1.04	95.92

From Table 2, it can be observed that the variance contribution ratio of the first two spatial modes is the highest, reaching 82.25% in cumulative variance contribution ratio. There is a sharp decrease in the variance contribution ratio of the third spatial mode, followed by a gradual decrease in the variance contribution ratio of all subsequent spatial modes. Therefore, it can be inferred that the main information of the sound field in the surveyed area is concentrated in the first two spatial modes. The cumulative variance contribution rate of the first seven spatial modes is 95.92%, which is greater than 95%. Therefore, it is decided to reconstruct the measured sound speed profiles using the first seven spatial modes.

(3) Reconstruction of measured sound speed profiles. Reconstruct the measured sound speed profiles according to Equation (7).

2. Method 2

(1) EOF decomposition. Combine the 42 historical sound speed profiles (excluding the tested sound speed profile) interpolated in Section 3.1 into a standard sound speed profile matrix. The average value of each row is then calculated to obtain the average sound velocity profile. In accordance with Section 2.2, the average sound velocity profile is concatenated with the measured sound velocity profile to obtain the sound velocity profile over the entire water depth. Following Section 2.1.1, EOF decomposition is performed on this matrix to obtain the first seven spatial modes as shown in Figure 10.

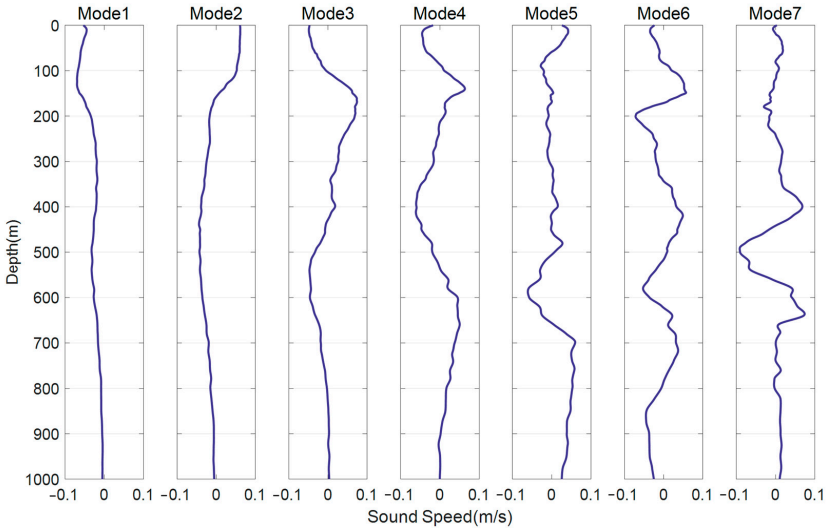

Figure 10. The first 7 spatial modes obtained from EOF decomposition of the standard sound velocity matrix.

(2) Determination of spatial mode order. The variance contribution ratio and cumulative variance contribution ratio of the first K spatial modes are calculated. The variation of the variance contribution ratio and cumulative variance contribution ratio for the first 20 spatial modes is shown in Figure 11, and the specific values of the variance contribution ratio and cumulative variance contribution ratio for the first seven spatial modes are shown in Table 3.

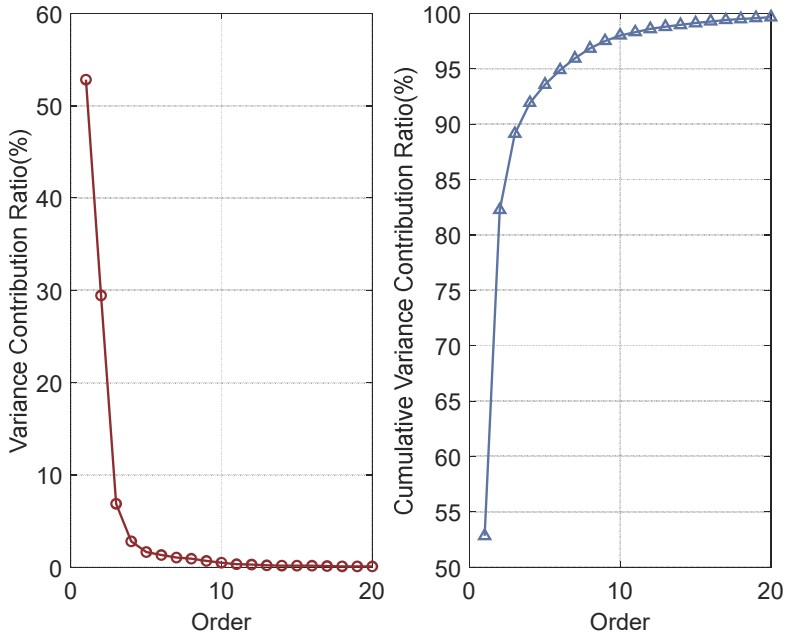

Figure 11. Variation of variance contribution ratio and cumulative variance contribution ratio of the first 20 spatial modes.

Table 3. Variance contribution ratio and cumulative variance contribution ratio of the first 7 spatial modes.

Mode	Eigenvalue	Variance Contribution Ratio (%)	Cumulative Variance Contribution Ratio (%)
1	1978.36	52.15	52.15
2	1138.46	30.01	82.16
3	265.35	6.99	89.15
4	108.29	2.85	92.00
5	58.68	1.55	93.55
6	50.22	1.32	94.87
7	39.04	1.03	95.90

Comparisons of Figures 9 and 11 and Tables 2 and 3 reveal that the trends in the variance contribution rate and cumulative variance contribution rate of each mode obtained by EOF decomposition using Method 1 and Method 2 are consistent, with only minor differences in numerical values. As the cumulative variance contribution rate of the first seven spatial modes is 95.90%, which exceeds 95%, the first seven spatial modes are chosen to reconstruct the measured sound velocity profile.

(3) Determination of upper and lower bounds for the CPO algorithm. The upper and lower bounds of the temporal coefficients corresponding to the first seven spatial modes are shown in Table 4.

Table 4. Upper and lower bounds of temporal coefficients corresponding to the first 7 spatial modes.

Mode	1	2	3	4	5	6	7
Upper Bound	71.42	76.94	37.33	22.85	15.28	15.75	18.48
Lower Bound	−92.15	−80.40	−42.00	−15.67	−22.16	−18.40	−16.19

The upper and lower bounds are arranged into 7-dimensional row vectors in ascending order of mode number, forming the upper and lower bounds of the algorithm search space.

(4) Initialization of algorithm parameters. According to Section 2.3.2, the population size is set to 40, the maximum number of iterations is set to 500, and the problem dimension is set to 7, representing the seven reconstruction coefficients to be obtained. The fitness function is set as the RMSE between the reconstructed sound velocity profile and the extrapolated measured sound velocity profile. After parameter initialization, the optimization process begins.

(5) Reconstruction of measured sound velocity profile. Following Equation (7), the measured sound velocity profile is reconstructed.

3.2.2. Constant Gradient Sound Ray Tracing and Accuracy Evaluation

In addition to various metric evaluations for the reconstructed sound velocity profile, it is imperative to validate its ability to meet the requirements for sound velocity correction. This underscores the significance of reconstructing the sound velocity profile, as it serves the purpose of multibeam bathymetry, with bathymetric accuracy being the ultimate criterion for assessment. There are several methods for sound velocity correction, such as the equivalent sound velocity profile method [34,35], average sound velocity method [36], and ray tracing method [37]. However, the prevailing multibeam bathymetric systems and post-processing software currently employ the constant gradient ray tracing method for the position calculation of sounding points. Despite its computational complexity, the constant gradient ray tracing method is widely adopted due to its high accuracy in sound velocity correction. The principles and computational methods of this method are detailed in reference [38] and will not be reiterated in this paper.

Regarding the maximum allowable error in bathymetry, the 6th edition of the International Hydrographic Organization (IHO) Standards for Hydrographic Surveys [39]

stipulates that for second-order depth measurements (in waters deeper than 200 m), the maximum error of sounding points at a 95% confidence level should not exceed 20 m plus 10% of the depth. The formula for calculating the depth error limit is as follows:

$$TVU_{max}(d) = \sqrt{a^2 + (b \times d)^2} \tag{13}$$

Here, TVU_{max}(m) represents the maximum allowable depth error, d(m) denotes the depth, a and b are coefficients. For second-order depth measurements, $a = 1.0$ (m), $b = 0.023$ (dimensionless coefficient).

The 2022 edition of the Chinese National Standard for Hydrographic Surveys specifies that for fourth-order surveys (in waters deeper than 200 m) or maps with scales smaller than 1:50,000, the maximum allowable error of sounding points at a 95% confidence level should not exceed 20 m, and the maximum allowable error in depth should not exceed 2% of the depth.

Both standards provide overall regulations for the positional and depth errors of sounding points but do not further refine the limits of errors caused by the sound velocity profile. The National Oceanic and Atmospheric Administration (NOAA) of the United States established in 1999 that a deviation exceeding 0.25% of the depth due to differences between the used sound velocity profile and the actual profile constitutes an over-limit condition. However, this regulation only restricts the depth error caused by the sound velocity profile and does not provide clarification on the positional errors it induces. Therefore, in the accuracy evaluation conducted in this study, NOAA's regulation is adopted for depth errors. Regarding positional errors, considering that the Chinese National Standard for Hydrographic Surveys is more stringent than the IHO Standards for Hydrographic Surveys and to ensure measurement accuracy, it is decided to adhere to the regulations of this standard.

We first simulate the generation of 131 beams, with a beam angle of 1° and an incidence angle ranging from $-60°$ to 60°. We then utilize the constant gradient sound ray tracing method to conduct ray tracing at various depths using reconstructed sound velocity profiles obtained from four different methods, and compare these results with the ray tracing outcomes using the tested sound velocity profile. This aims to assess the efficacy of the sound velocity corrections at different depths as furnished by the reconstructed sound velocity profiles.

3.3. Evaluation Metrics

To comprehensively evaluate the reconstruction performance of each method, RMSE (Root Mean Squared Error), MAE (Mean Absolute Error), MAPE (Mean Absolute Percentage Error), and R^2 (R-squared) are selected as evaluation metrics. RMSE measures the magnitude of the reconstruction error, i.e., the difference between the reconstructed values and the true values. A smaller RMSE indicates better consistency between the reconstructed and true values. This metric is sensitive to large errors and can effectively reflect the model's ability to handle outliers or extreme values. MAE quantifies the average magnitude of differences between reconstructed and true values. Although it is less sensitive than RMSE, it provides a more intuitive result, with smaller values indicating better model performance. MAPE measures the relative error between reconstructed and true values, reflecting the extent to which reconstructed values deviate from true values. Smaller MAPE values indicate better reconstruction performance of the model. R^2 measures the model's fitting ability to the data. It is a dimensionless metric ranging from 0 to 1, with values closer to 1 indicating better model fitting performance. The formulas for calculation are as follows:

$$RMSE = \sqrt{\frac{1}{\mathrm{n}}\sum_{i=1}^{n}(\hat{y}_i - y_i)^2} \tag{14}$$

$$MAE = \frac{1}{n}\sum_{i=1}^{n}|\hat{y}_i - y_i| \tag{15}$$

$$MAPE = \frac{1}{n}\sum_{i=1}^{n}\left|\frac{\hat{y}_i - y_i}{y_i}\right| \times 100\% \tag{16}$$

$$R^2 = 1 - \frac{\sum_{i=1}^{n}(\hat{y}_i - y_i)^2}{\sum_{i=1}^{n}(\overline{y} - y_i)^2} \tag{17}$$

Here, y_i represents the sound velocity value at the i depth in the measured sound velocity profile, $\hat{y}_i$ represents the sound velocity value at the i depth in the reconstructed sound velocity profile, $\overline{y}$ represents the average sound velocity in the measured sound velocity profile, and n represents the number of sound velocity points.

4. Results and Discussion

4.1. Analysis of Reconstruction Results with Fixed Sampling Depth of the Measured Sound Speed Profile

During the experiment, the sampling depth of the measured sound speed profile was set to 200 m, and four methods were employed to reconstruct it. Both Method 1 and Method 2 as proposed in this paper are based on the principle of EOF. The reconstruction coefficients obtained by the two methods are shown in Table 5, indicating that the coefficients obtained by both methods are generally consistent.

Table 5. Reconstruction coefficients obtained by Method 1 and Method 2 for sound speed profile.

Order	1	2	3	4	5	6	7
Method 1	52.8544	1.4062	6.0237	−0.1497	−13.4213	5.1578	−8.0620
Method 2	51.8908	1.2862	5.9058	−0.1643	−14.8596	3.7157	−6.6353

The reconstructed sound speed profiles and corresponding metrics for each method are shown in Figure 12 and Table 6, respectively.

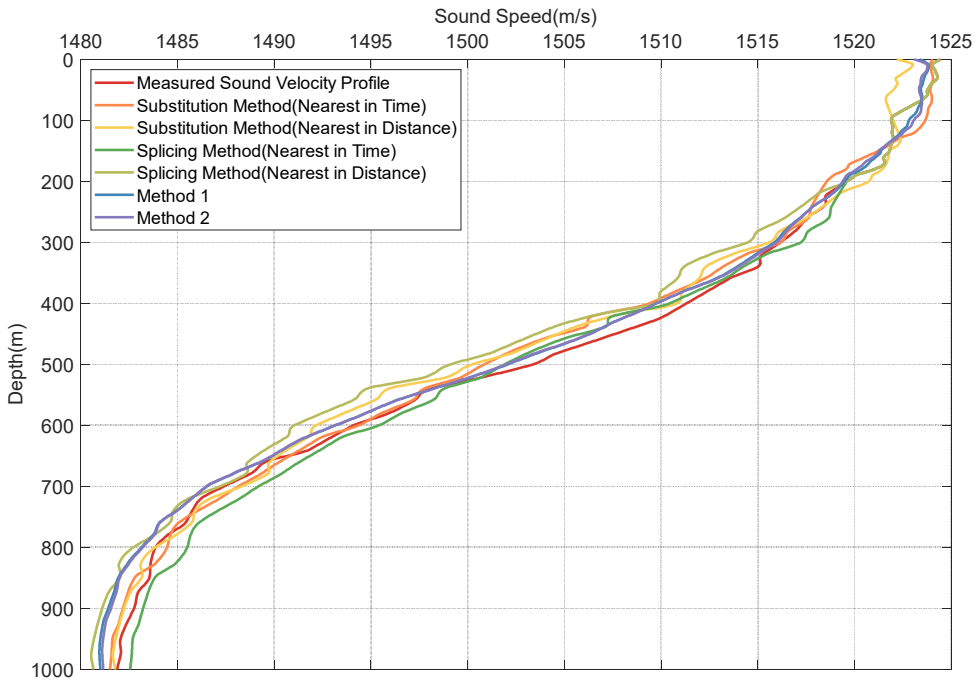

Figure 12. Reconstructed sound speed profiles obtained by four methods.

Table 6. RMSE, MAE, MAPE, and R^2 of each reconstructed sound speed profile.

	Nearest Substitution Method		Nearest Splicing Method		Method 1	Method 2
	Time Nearest	Location Nearest	Time Nearest	Location Nearest		
RMSE (m/s)	1.1938	1.3802	0.9975	2.0551	0.9594	0.9511
MAE (m/s)	0.8638	1.0548	0.7739	1.5959	0.8510	0.8492
MAPE (%)	0.0574	0.0701	0.0517	0.1064	0.0568	0.0566
R^2	0.9942	0.9922	0.9959	0.9827	0.9962	0.9963

From Table 6, it can be observed that for the measured sound speed profile with a sampling depth of 200 m used in this experiment, Method 2 achieves RMSE, MAE, MAPE, and R2 for the full-depth (1000 m) reconstructed sound speed profile of 0.9511 m/s, 0.8492 m/s, 0.0566%, and 0.9963, respectively. These metrics surpass those of other methods, signifying that Method 2 can more precisely depict the sound speed profile across the entire water depth, leveraging the measured sound speed profile at a specific location. While Method 1's performance across various metrics is marginally inferior to that of Method 2, the disparities are negligible. In contrast to the nearest substitution and nearest splicing approaches, Method 1 maintains evident superiority. The nearest substitution and nearest splicing approaches do not exhibit absolute superiority or inferiority between them. For each approach individually, utilizing the sound speed profile closest in time yields superior reconstruction effects compared to employing the sound speed profile nearest in location. Importantly, the RMSE of the reconstructed sound speed profile, acquired by splicing the nearest sound speed profile in location with the measured one, stands at 2.0551 m/s, markedly exceeding the corresponding value for other reconstructed profiles. This occurs because during the splicing process, the difference between the sound speed at the end of the measured sound speed profile and the sound speed at the same depth of the spliced sound speed profile needs to be calculated and added to all sound speeds of the spliced sound speed profile that are deeper than the sampling depth. As shown in Figure 12, the sound speed profile nearest in location is closer to the tested sound speed profile originally, but after adding the difference, the profile shifts to the left, away from the tested sound speed profile, leading to increased error. Therefore, whether nearest in time or nearest in location, the splicing approach may confront these issues, potentially yielding errors surpassing those of direct substitution. Only when the sound speed trends of two points align or the disparity in sound speed remains minimal can the splicing approach yield superior outcomes. Nevertheless, predicting sound speed fluctuations between two points proves unfeasible in practice. Thus, in regard to stability, the method advanced in this study also holds merit.

The sound speed error curves of different depths of each reconstructed sound speed profile are shown in Figure 13, and the corresponding statistical parameters are shown in Table 7.

Table 7. Statistical parameters of sound speed errors for each reconstructed sound speed profile.

	Nearest Substitution Method		Nearest Splicing Method		Method 1	Method 2
	Time Nearest	Location Nearest	Time Nearest	Location Nearest		
Maximum (m/s)	3.7194	3.1448	2.6747	4.2695	1.9417	1.9325
Minimum (m/s)	−1.7867	−1.1246	−2.0204	0	−1.0022	−1.2678
Mean (m/s)	0.5180	0.8037	−0.3053	1.5959	0.7673	0.7445

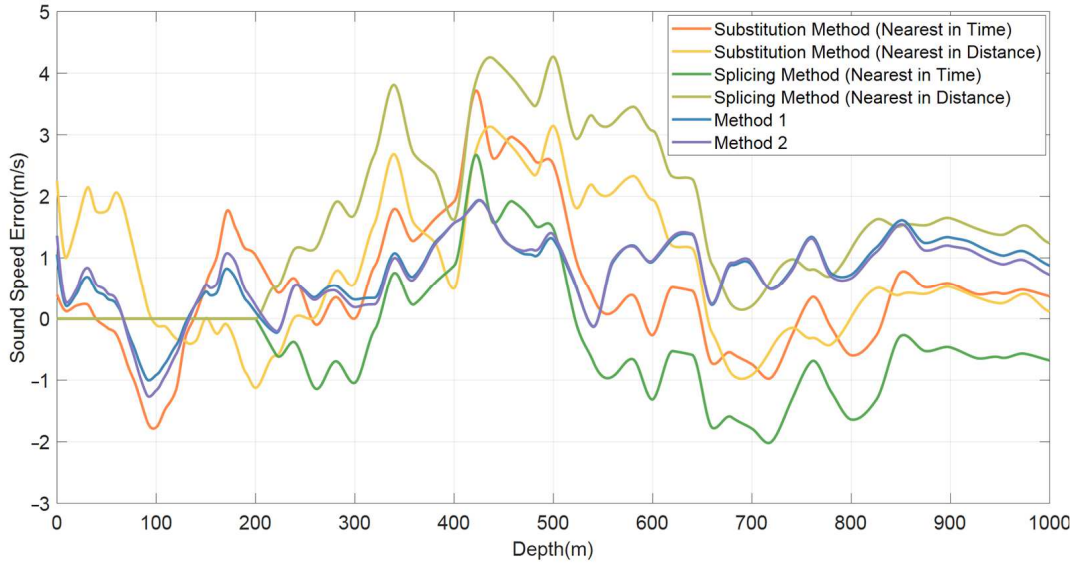

Figure 13. Sound speed error curves of each reconstructed sound speed profile.

Figure 14 illustrates that the sound speed errors of both Method 1 and Method 2 range from 0–2 m/s, with more than half of the errors falling below 1 m/s. When splicing the sound speed profile nearest in time with the measured sound speed profile, although 69% of sound speed errors are less than 1 m/s, 3% of sound speed errors are distributed between 2–3 m/s, resulting in inferior reconstruction results compared to Method 1 and Method 2. When substituting the measured sound speed profile with the sound speed profile nearest in time, 72% of sound speed errors are less than 1 m/s, which is the highest proportion among all reconstructed sound speed profiles. However, this method generates a wide range of sound speed errors, ranging from 0–4 m/s, leading to unsatisfactory reconstruction results. The method of splicing the sound speed profile nearest in location performs the worst, as evident from the figure, characterized by the broadest range of error distribution. According to Table 7, the maximum sound speed error reaches 4.2695 m/s.

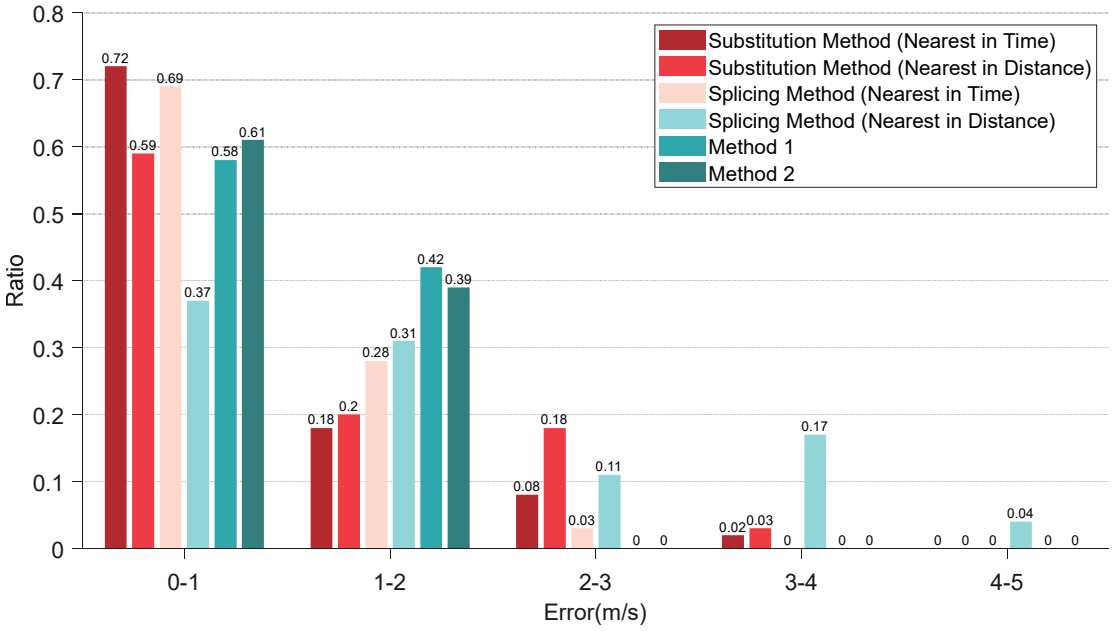

Figure 14. Distribution of sound speed errors for each reconstructed sound speed profile. The *x*-axis represents the range of sound speed errors, and the *y*-axis represents the ratio of sound speed points, whose errors fall within a certain range, to the total number of sound speed points in the sound speed profile.

4.2. Analysis of Reconstruction Results with Variable Sampling Depth of the Measured Sound Speed Profile

The analysis in Section 4.1 is conducted based on a measured sound speed profile with a sampling depth of 200 m. In order to comprehensively evaluate the performance of each method under different sampling depths of the measured sound speed profile, sampling depths are set from 0 m to 1000 m at intervals of 1 m. RMSE is employed as the evaluation metric. The performance of each method under varying sampling depths is depicted in Figure 15.

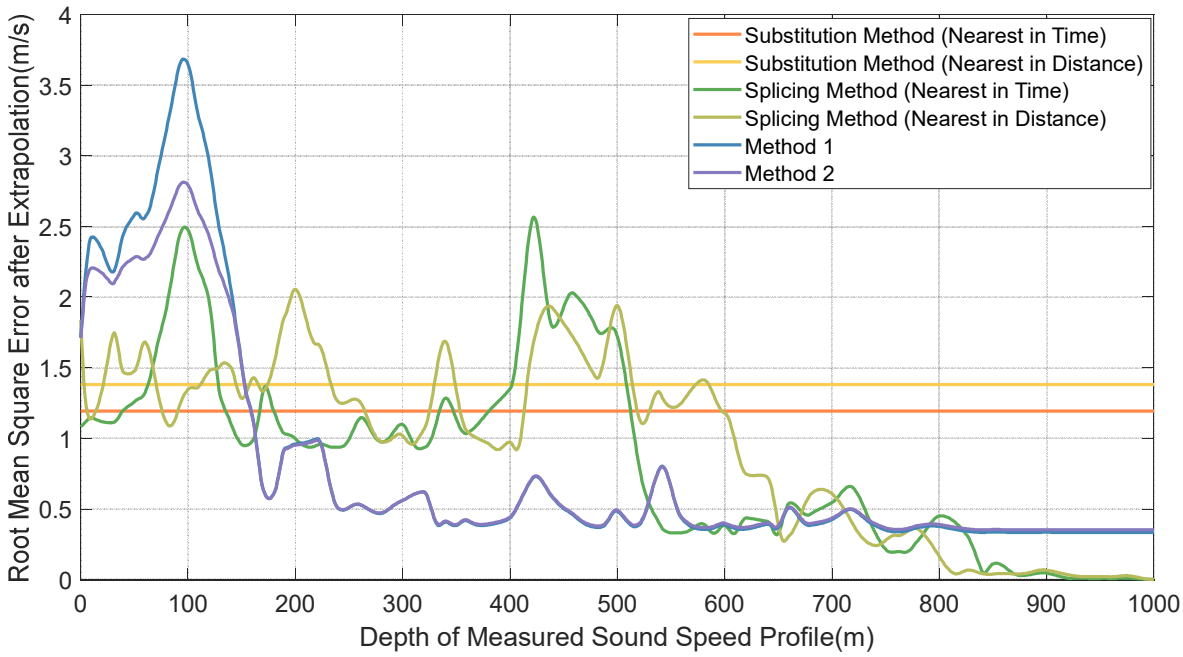

Figure 15. Performance of each method in reconstructing sound speed profiles with variable sampling depths.

Examination of Figure 15 reveals that for sampling depths of the measured sound speed profile below 152 m, both Method 1 and Method 2 demonstrate suboptimal reconstruction efficacy relative to the nearest substitution and nearest splicing methodologies. Method 1 exceeds an RMSE of 3.5 m/s, showcasing the least favorable performance among all methodologies. Conversely, Method 2 surpasses Method 1, with its efficacy steadily ameliorating as the sampling depth extends past 100 m. Upon reaching a depth of 147 m, both Method 1 and Method 2 commence demonstrating nearly indistinguishable efficacy, sustaining consistent performance with increasing sampling depth. Upon reaching a depth of 162 m, both methodologies surpass the substitution and splicing approaches, attaining an RMSE of under 1 m/s in sound speed profile reconstruction. This performance gradually stabilizes, providing a reference for determining the sampling depth of the measured sound speed profile. Combining this analysis with Figure 8, it is observed that the significant variations in the spatial modes occur predominantly within depths ranging from 100 m to 200 m. As the sampling depth of the measured sound speed profile surpasses this layer, the reconstruction performance of both Method 1 and Method 2 improves. Therefore, it is recommended that to attain satisfactory reconstruction outcomes, the sampling depth of the measured sound speed profile ideally should surpass the depths harboring substantial spatial mode variations, which are typically situated within shallow water layers.

4.3. Analysis of Sound Ray Tracing Results

To enhance computational efficiency, sound ray tracing was initiated at a depth of 50 m, with intervals of 25 m until the maximum water depth (1000 m) was reached. The results of sound ray tracing for the four methods indicate that except for the substitution method (location nearest), which exhibited some instances of edge beam measurements

exceeding the limit, the methods all met the accuracy requirements proposed in Section 3.2.2 and the effective beam ratio reached 100%. Regarding the effective beam ratio, Zhu Xiaochen [40] pointed out in his doctoral dissertation that it represents the ratio of beams meeting the depth tolerance to the total number of beams, quantifying the effectiveness of sound speed correction for multibeam measurement data. It is worth noting that, in Table 6, the metrics of the substitution method (location nearest) are actually superior to those of the splicing method (location nearest). However, the results of sound ray tracing for the substitution method (location nearest) are inferior to those of the splicing method (location nearest). The reason is that, in the shallower part of the splicing depth, the sound speed profile nearest in location differs significantly from the actual sound speed profile (as shown in Figure 12). During sound ray tracing, errors accumulate layer by layer. In contrast, the splicing method matches the actual sound speed profile in the shallower depths, resulting in no errors during sound ray tracing in this layer. Although the difference between the splicing method and the actual sound speed profile is greater in the deeper part of the splicing depth compared to the substitution method, the absence of error accumulation in the shallower part results in higher overall tracking accuracy for the splicing method.

Figure 16 illustrates the sound ray tracing errors for Methods 1 and 2, including depth errors and position errors of depth measurement points. The trends of sound ray tracing errors for each method are similar. Due to space limitations, this paper specifically analyzes only the sound ray tracing errors of Method 2.

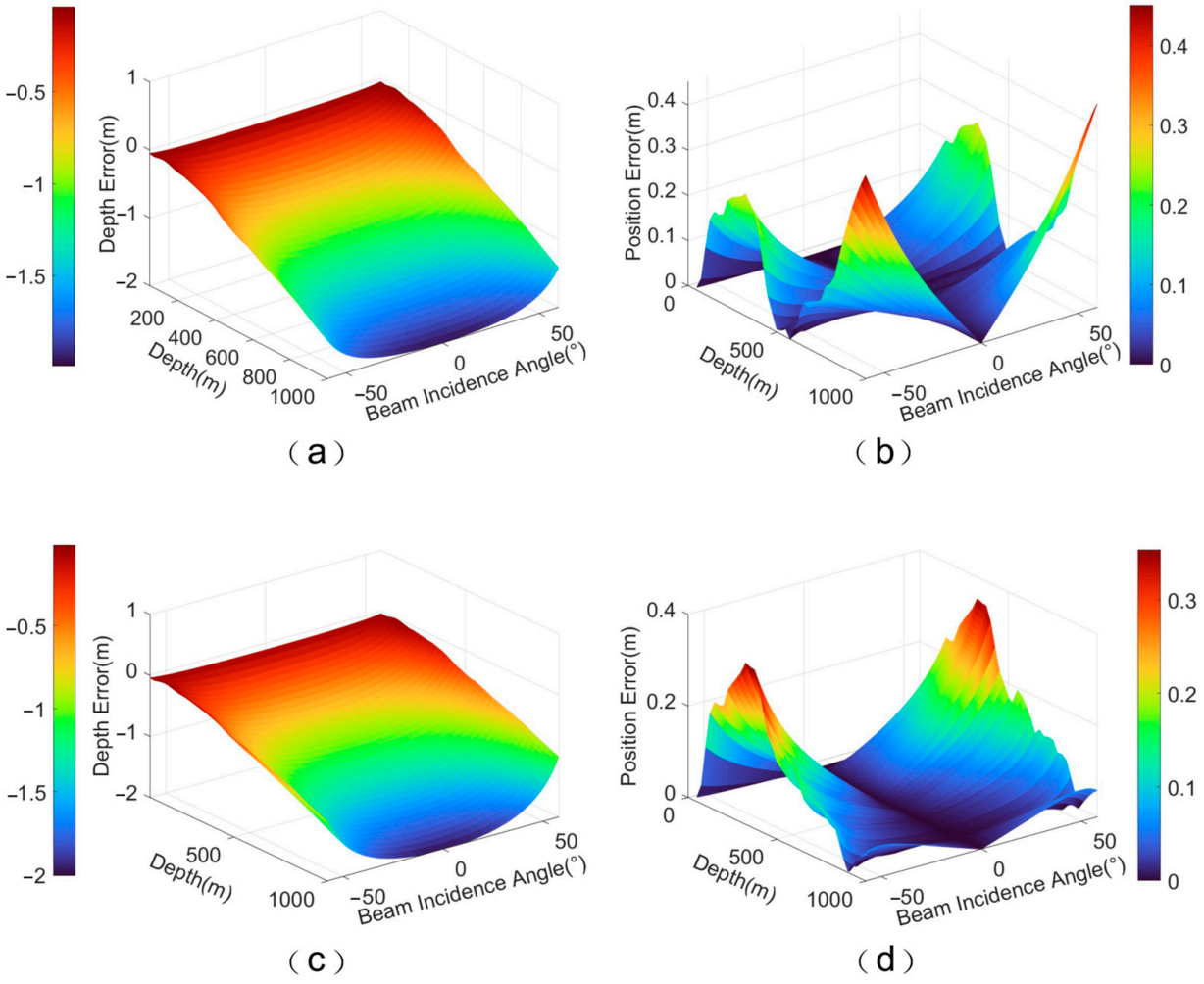

Figure 16. Sound ray tracing results for Methods 1 and 2. (**a**) Depth error for Method 1. (**b**) Position error for Method 1. (**c**) Depth error for Method 2. (**d**) Position error for Method 2.

Figure 16c depicts the depth errors of sound ray tracing for Method 2. Here, "depth error" refers to the absolute difference between the sound speed correction mutual difference of the actual sound speed profile and the reconstructed sound speed profile and 0.25% of the water depth value. If this value is less than 0, it indicates that the sound speed correction results of the reconstructed sound speed profile meet the measurement accuracy requirements. Overall, as the depth increases, the mutual difference in depth becomes increasingly smaller than 0.25% of the water depth, indicating that the deeper the water, the closer the sound ray tracing results using the reconstructed sound speed profile are to the sound ray tracing results of the actual sound speed profile. When the depth is constant, as the incident angle of the beam increases, the depth error gradually increases, and the sound ray tracing results of edge beams are significantly inferior to those of central beams.

Figure 16d illustrates the position errors of sound ray tracing for Method 2. Compared to depth errors, position errors do not exhibit a singular trend of increasing or decreasing with depth. Instead, they fluctuate, indicating that at certain depths, the sound ray tracing results are better. However, for any depth, the position error is far below the accuracy indicators proposed in Section 3.2.2.

5. Conclusions

During the execution of a deep-sea multibeam bathymetric survey, the acquisition of representative sound speed profiles for the surveyed sea areas emerges is a pivotal task, indispensable for guaranteeing the quality of the collected data. Nonetheless, the acquisition of full-depth sound speed profiles presents formidable challenges, owing to factors encompassing the effective detection depth of equipment, meteorological conditions, variations in seabed topography, and operational efficiency considerations. The variation of sound speed in seawater, though intricate, still exhibits discernible regularities on specific spatiotemporal scales within the remote ocean. To tackle this complexity, an approach that involves leveraging a substantial dataset consisting of historical full-depth sound speed profiles obtained from maritime regions is proposed. Through the application of EOF analysis, the aim is to identify the underlying patterns of variability, which can facilitate the reconstruction of partially-depth measured sound speed profiles. To mitigate the limitation of EOF reconstruction depth posed by the shallowest historical sound speed profiles, the measured sound speed profile is integrated with the historical mean sound speed profile to create comprehensive full-depth representations. Building upon this framework, two methodologies are presented for reconstructing the measured sound speed profile.

In the experiments utilizing Argo data, the sampling depth of the measured sound speed profile is set at 200 m. Method 1 and Method 2 are compared with commonly used methods in practical measurements, such as the substitution method and the splicing methods. The experimental results indicate that Method 2 outperforms other methods, yielding a reconstructed sound speed profile with superior performance. This is evidenced by lower RMSE, MAE, MAPE, and higher R2 values compared to the alternatives. While Method 1 shows slightly inferior performance to Method 2, the discrepancies between the two methods are negligible, and both notably surpass the substitution and splicing methods. It is important to note that the efficacy of the substitution and splicing methods heavily relies on the hydrological conditions of the surveyed sea area.

Further experimentation involving varying depths of the measured sound speed profile reveals that Method 1 and Method 2 exhibit decreased effectiveness compared to the substitution method and the splicing methods when the measured sound speed profile is shallow. However, the experimental results demonstrate that that once the depth of the measured sound speed profile surpasses the depths where the primary spatial modes undergo significant changes, the performance of Method 1 and Method 2 improves significantly. It is recommended that measurement operators take this depth into consideration when determining the measurement depth of the sound speed profile. Compared to the current measurement depth, which typically extends to at least the depth where the sound

channel axis appears (approximately 1000–1500 m), this optimized depth is considerably reduced, thereby enhancing operational efficiency significantly.

Finally, sound ray tracing of reconstructed sound speed profiles is conducted at different depths. Apart from the substitution method (location nearest) which exhibits some instances of edge beam measurements exceeding the limit, all the other methods meet the measurement accuracy requirements, with an effective beam ratio of 100%.

In future research, we will focus on improving the performance of the proposed methods in reconstructing sound speed profiles when the sampling depth is shallow and explore other methods with superior performance for sound speed profile reconstruction.

Author Contributions: Conceptualization, S.J.; Methodology, W.Z.; Formal analysis, G.B.; Resources, C.P. and H.X.; Writing—original draft, W.Z.; Writing—review & editing, S.J. All authors have read and agreed to the published version of the manuscript.

Funding: This research received no external funding.

Institutional Review Board Statement: Not applicable.

Informed Consent Statement: Not applicable.

Data Availability Statement: Data are contained within the article.

Conflicts of Interest: The authors declare no conflict of interest.

References

1. Li, J. *Multibeam Survey Principles, Techniques and Methods*; Ocean Press: Beijing, China, 1999; ISBN 7-5027-4834-2.
2. He, G.W.; Liu, F.L.; Yu, P.; Yang, S.X.; Zhang, Z.R.; Zhao, Z.B. Sound Velocity Correction of Multibeam Bathymetric Systems. *Mar. Geol. Quat. Geol.* **2000**, *4*, 109–114. [CrossRef]
3. Dong, Q.L.; Han, H.Q.; Fang, Z.B.; Pan, L.; Chen, Y.Y.; Lu, G.F. The Influence of Sound Speed Profile's Correction on Multibeam Survey. *Hydrogr. Surv. Charting* **2007**, *27*, 56–58.
4. Li, J.B.; Zheng, Y.L.; Wang, X.B.; Wu, Z.Y. Main Factors Affecting Multibeam Bathymetric Survey Accuracy. *Hydrogr. Surv. Charting* **2001**, 26–32. Available online: https://kns.cnki.net/KCMS/detail/detail.aspx?dbcode=CJFD&dbname=CJFD2001&filename=HYCH200101005&v= (accessed on 21 March 2024).
5. Liu, S.X.; Qu, X.J.; Gao, P.L. New New Idea for the Accuracy of Multibeam Affected by SVP. *Hydrogr. Surv. Charting* **2008**, *28*, 31–34.
6. Zhao, J.H.; Liu, J.N. *Multibeam Bathymetric Survey and Image Data Processing*; Wuhan University Press: Wuhan, China, 2008; ISBN 978-7-307-06500-0.
7. Meng, S. Discussion on the Influence of Sound Velocity on Multibeam Bathymetric Measurement and Countermeasures. *Ship Supplies Mark.* **2019**, *6*, 20–21. [CrossRef]
8. Huang, C.H.; Zhang, W.D.; Zhang, Q.L.; Wang, C.; Shen, J.S.; Lu, X.P.; Huang, X.Y. Reconstruction of Full-depth Sound Velocity Profile by Joint WOA2018 Temperature-Salinity Model and In-situ Temperature-Salinity Data (I): Demand Analysis and Technical Scheme. *Mar. Surv.* **2020**, *40*, 24–29.
9. Zhang, Q.G.; Chen, X.; Liu, Q. Research on Sound Velocity Profile Acquisition Method in Remote Multibeam Bathymetric Survey. *Mar. Surv.* **2019**, *39*, 1–4.
10. Huang, C.H.; Lu, X.P.; Ye, A.N.; Luo, S.R.; Huang, X.Y.; Ge, Z.X. Quality Check and Evaluation of Seafloor Topography Measurement Results (II): Acquisition of Sound Velocity Profiles in Deep-sea Areas. *Mar. Surv.* **2017**, *37*, 12–16+20.
11. Zhang, Y.F.; Cheng, D.; Li, S.Q.; Wu, D.S. Research on Sound Velocity Profile Acquisition Method in Deep-sea Areas with Multi-beam Bathymetric Survey. *Mar. Surv.* **2020**, *40*, 27–31.
12. NOAA. *NOS Hydrographic Surveys Specifications and Deliverables*; NOAA: Silver Spring, MD, USA, 2021.
13. Huang, C.H.; Wang, Z.; Zhang, X.J.; Yao, J.J.; Li, Z.Q.; Shen, J.S.; Lu, X.P. Reconstruction of Full-depth Sound Velocity Profile by Joint WOA2018 Temperature-Salinity Model and In-situ Temperature-Salinity Data (II): Accuracy Evaluation. *Mar. Surv.* **2020**, *40*, 9–14.
14. Kammerer, E. A New Method for the Removal of Refraction Artifacts in Multibeam Echosounder Systems. Doctoral Dissertation, University of New Brunswick, Fredericton, NB, Canada, 2000.
15. Wu, T.Y.; Xiao, F.M.; Liu, Y.C.; Zhu, X.C. The Method for Sound Velocity Profile Extrapolation. In Proceedings of the China Society of Surveying and Mapping, Marine Surveying and Mapping Professional Committee, Chengdu, China, 13 September 2009; pp. 227–230. Available online: https://kns.cnki.net/KCMS/detail/detail.aspx?dbcode=CPFD&dbname=CPFD0914&filename=CMJH200909001058&v= (accessed on 21 March 2024).
16. Munk, W.H. Sound Channel in an Exponentially Stratified Ocean, with Application to SOFAR. *J. Acoust. Soc. Am.* **1974**, *55*, 220–226. [CrossRef]

17. Davis, T.M.; Count, R.; Yman, K.A.; Carron, M.J. Tailored Acoustic Products Utilizing the NAVOCEANO GDEM (a Generalized Digital Environmental Model). In Proceedings of the 36th Naval Symposium on Underwater Acoustics, San Diego, CA, USA, 1–3 April 1986; pp. 127–131.
18. Zhang, X.; Zhang, Y.G.; Zhang, J.X.; Dong, N. A New Parametric Method for Sound Velocity Profile. *Acta Oceanol. Sin. (Chin. Ed.)* **2011**, *33*, 54–60. [CrossRef]
19. LeBlanc, L.R.; Middleton, F.H. An Underwater Acoustic Sound Velocity Data Model. *J. Acoust. Soc. Am.* **1980**, *67*, 2055–2062. [CrossRef]
20. Park, J.C.; Kennedy, R.M. Remote Sensing of Ocean Sound Speed Profiles by a Perceptron Neural Network. *IEEE J. Ocean. Eng.* **1996**, *21*, 216–224. [CrossRef]
21. Shen, Y.H.; Ma, Y.L.; Tu, Q.P.; Jiang, X.Q. Feasibility Study of Representing Shallow Water Sound Velocity Profile Using Empirical Orthogonal Functions (EOF). *Appl. Acoust.* **1999**, *18*, 21–25.
22. Sun, W.C.; Bao, J.Y.; Jin, S.H. Impact of EOF Representation of Sound Velocity Profile on Multibeam Bathymetric Data. *Mar. Surv.* **2014**, *34*, 21–24+28.
23. He, L.; Li, Z.L.; Zhang, R.H.; Li, F.H. Empirical Orthogonal Function Representation and Matching Field Inversion of Sound Velocity Profile in East China Sea. *Prog. Nat. Sci.* **2006**, *16*, 351–355.
24. Zhang, Z.M.; Li, Z.L.; Dai, Q.X. Reconstruction of Full-depth Sound Velocity Profile Using Limited-depth Sound Velocity Data. In Proceedings of the 2008 National Acoustics Conference, Shanghai, China, 22–24 October 2008; p. 2. Available online: https://kns.cnki.net/kcms2/article/abstract?v=p7sfyaWOx3OSCy4rHJ9BblVKlFiMvVsmNEAz0a-IYxHD5Kik5UeHLi7FfvKDR75fC2IKhu3gA9IoNous9oypI2tmZOvOFg7_ZZfYkWntGBK3mSsWrdYeSyjy-lch7GeMuIcUHuRZC12CH00gCG1uVw==&uniplatform=NZKPT&language=CHS (accessed on 21 March 2024).
25. Zhang, W.; Huang, Y.W.; Wang, Y.Y. Reconstruction of Sound Velocity Profile Using Incomplete Sample Data. *Acoust. Tech.* **2012**, *31*, 371–374.
26. Cheng, F.; Chen, S.; Jin, S.H.; Sun, W.C. Study on Extrapolation Method of Sound Velocity Profile in Continental Margin Deep Water Area. *Mar. Surv.* **2016**, *36*, 26–29.
27. Yang, F.; Zheng, H.; Zheng, H.; Wang, J.; Kong, L.M.; Xu, K. Analysis of Sound Velocity Structure and Empirical Orthogonal Function Extension in Zhoushan Sea Area. *China Water Transp.* **2016**, *16*, 142–144.
28. Pearson, K. On Lines and Planes of Closest Fit to Systems of Points in Space. *Lond. Edinb. Dublin Philos. Mag. J. Sci.* **1901**, *2*, 559–572. [CrossRef]
29. Davis, R.E. Predictability of Sea Surface Temperature and Sea Level Pressure Anomalies over the North Pacific Ocean. *J. Phys. Oceanogr.* **1976**, *6*, 249–266. [CrossRef]
30. Nie, G.G.; Wan, J.H. Application of Akima Interpolation Method in Measurement. *Surv. Technol. News* **1998**, 31–34. Available online: https://kns.cnki.net/kcms2/article/abstract?v=6xaVI2TORM3dHWE9xfyhgc32MqFWacD09temugaiNPMKdrIL9q3lhHKiKPOk7rD2YXP-oJbiPzLOdm57cRLlvtWrpCz8tajgWLsxHs5IWEBvh04ne-b5Vs0N8GMXy9hW4r3iwk1A-c0=&uniplatform=NZKPT&language=CHS (accessed on 21 November 2023).
31. Bica, A.M. Optimizing at the End-Points the Akima's Interpolation Method of Smooth Curve Fitting. *Comput. Aided Geom. Des.* **2014**, *31*, 245–257. [CrossRef]
32. Abdel-Basset, M.; Mohamed, R.; Abouhawwash, M. Crested Porcupine Optimizer: A New Nature-Inspired Metaheuristic. *Knowl.-Based Syst.* **2024**, *284*, 111257. [CrossRef]
33. Zhou, F.N.; Zhao, J.H.; Zhou, C.Y. Determination of Classic Experiential Sound Speed Formula in Multibeam Echo Sounding System. *J. Oceanogr. Taiwan Strait* **2001**, *20*, 411–419.
34. Ding, J.S.; Zhou, X.H.; Tang, Q.H.; Liu, Z.C.; Chen, Y.L. Correction Technique of Sound Ray Refraction for Multibeam Echo Sounder System Based on Equivalent Sound Velocity Profile Method. *Hydrogr. Surv. Charting* **2004**, *24*, 27–29.
35. Fang, W.M. Research on Sound Velocity Correction Method Based on Equivalent Sound Velocity Profile Method and Its Improved Model. *China Water Transp.* **2013**, *13*, 72–73.
36. Wang, J. Research on Sound Velocity Correction Method for Multibeam Echo Sounder. Master's Thesis, China University of Petroleum (East China), Qingdao, China, 2012.
37. Qi, N.; Tian, T. Sound Ray Tracking Technology in Multibeam Swath Bathymetry. *J. Harbin Eng. Univ.* **2003**, *24*, 245–248.
38. Lu, X.P.; Bian, S.F.; Huang, M.T.; Zhai, G.J. Improved Algorithm for Average Sound Velocity in Constant Gradient Sound Ray Tracking. *J. Wuhan Univ. (Inf. Sci. Ed.)* **2012**, *37*, 590–593. [CrossRef]
39. IHO. *IHO Standards for Hydrographic Surveys*, 6th ed.; Special Publication No. 44; IHO: Monaco City, Monaco, 2020.
40. Zhu, X.C. *Research on Key Models and Applications of Multibeam Echo Sounder Data Processing*; Dalian Naval Academy: Dalian, China, 2011.

Disclaimer/Publisher's Note: The statements, opinions and data contained in all publications are solely those of the individual author(s) and contributor(s) and not of MDPI and/or the editor(s). MDPI and/or the editor(s) disclaim responsibility for any injury to people or property resulting from any ideas, methods, instructions or products referred to in the content.